THE JOURNAL OF PHYSICAL CHEMISTRY Letters

Letter

pubs.acs.org/JPCL

Interpretation of Cyclic Voltammetry Measurements of Thin Semiconductor Films for Solar Fuel Applications

Luca Bertoluzzi, Laura Badia-Bou, Francisco Fabregat-Santiago, Sixto Gimenez, and Juan Bisquert*

Photovoltaics and Optoelectronic Devices Group, Departament de Física, Universitat Jaume I, 12071 Castelló, Spain

Supporting Information

ABSTRACT: A simple model is proposed that allows interpretation of the cyclic voltammetry diagrams obtained experimentally for photoactive semiconductors with surface states or catalysts used for fuel production from sunlight. When the system is limited by charge transfer from the traps/catalyst layer and by detrapping, it is shown that only one capacitive peak is observable and is not recoverable in the return voltage scan. If the system is limited only by charge transfer and not by detrapping, two symmetric capacitive peaks can be observed in the cathodic and anodic directions. The model appears as a useful tool for the swift analysis of the electronic processes that limit fuel production.

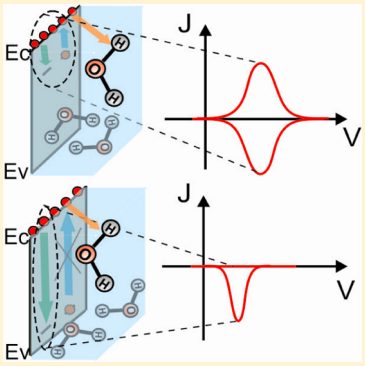

SECTION: Energy Conversion and Storage; Energy and Charge Transport

Direct transformation of solar energy into chemical energy by hydrogen production through water splitting with semiconductor materials in a photoelectrochemical cell constitutes an attractive solution to our energy needs. However, despite the intense efforts carried out in the last decades, no single material has been identified satisfying all of the efficiency, stability, and cost conditions needed for industrial deployment of this technology.[1−4]

Hematite (α-Fe_2O_3) has emerged as a promising candidate[5−9] due to its abundance in the earth crust, visible light absorption, and good stability in the harsh environmental conditions needed for operation, although the obtained solar-to-fuel efficiencies still remain low for commercial exploitation. One of the main causes of the low performance of hematite is related to the large overpotentials required for water oxidation (around 500 mV), and surface treatments have proven to enhance notably water splitting performances.[10−12] It has been suggested that the reasons for these large overpotentials are related to sluggish hole transfer to the electrolyte[13,14] and to the existence of traps in the bulk and at the semiconductor/electrolyte interface,[15−17] leading to high recombination.[18,19] Clearly, the separation of the different processes that constitute the oxidative current and the identification of the main kinetic bottlenecks are complex tasks. Therefore, the accurate interpretation of the results provided by characterization techniques constitutes a key tool to rationalize materials development and device optimization. Recently, we have proposed a simple physical model that allows the interpretation of impedance spectroscopy (IS) spectra for water splitting applications.[20] In this model, we have considered a monoenergetic level of surface states where both electron and holes can recombine or transfer from/to the solution.

In the present study, we propose a complementary simple model to predict the curves obtained by cyclic voltammetry (CV). This characterization technique allows a quick test of the faradic behavior associated with charge transfer and the capacitive behavior associated with the separated modes of carrier storage, which depend on the thermodynamics and kinetics of the system at stake.[21] Starting from the characteristic features of reported voltammograms of hematite and related systems, we have derived a model that is able to map the different kinetic configurations of a system used for solar fuel applications. We show that two types of peaks featuring charge storage in traps can be observed when charge transfer from surface states is kinetically limited. Those peaks allow characterization of the degree of recombination at the surface states and are discussed below.

In Figure 1, we present the typical voltammetry plots obtained for an Fe_2O_3 sample synthetized by atmospheric pressure chemical vapor deposition (APCVD).[22,23] Figure 1a shows the effect of a pretreatment in dark conditions at different anodic potentials V_0 during 60 s. The voltammetry plots were recorded at a fixed scan rate (500 mV/s). This figure displays a clear cathodic capacitive peak whose height increases as the pretreatment anodic potential increases. A linear dependence exists between the peak current and V_0, as can be seen in Figure 1b. This peak can be attributed to the charging of a monoenergetic level of surface states. It can be remarked that at a low potential (here, V_0 = 1.66 V versus

Received: March 13, 2013
Accepted: April 5, 2013

dx.doi.org/10.1021/jz400573t | J. Phys. Chem. Lett. 2013, 4, 1334−1339

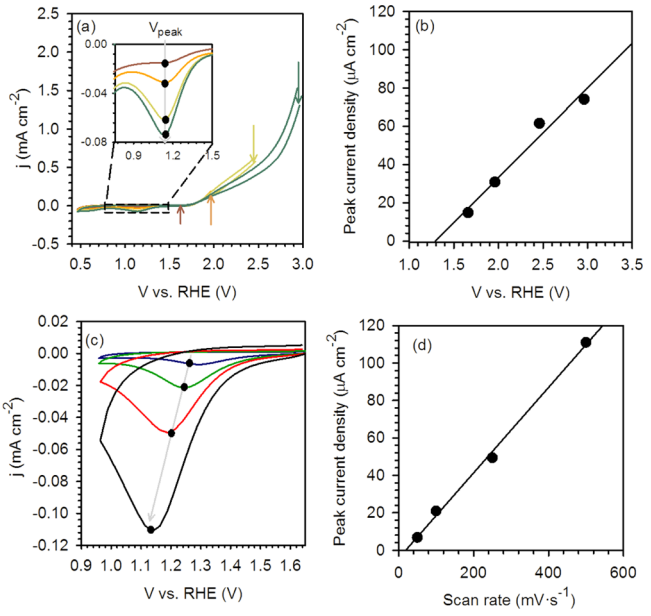

Figure 1. (a) Voltammogram of Fe_2O_3 in the dark after 60 s of pretreatment at different static potentials V_0 (indicated by arrows) at a fixed scan rate of s = 0.5 V s^{-1}. Each capacitive peak occurs at the same voltage peak V_{peak} = 1.14 V versus RHE. Absolute values of the capacitive peaks: j_1 = 13 μA cm^{-2}, j_2 = 31 μA cm^{-2}, j_3 = 62 μA cm^{-2}, and j_4 = 74 μA cm^{-2} (b) Peak current versus voltage extracted from (a). (c) Voltammogram of Fe_2O_3 in the dark after 60 s of pretreatment under 1 sun illumination at V_0 = 1.66 V versus RHE and different scan rates (50, 100, 250, and 500 mV s^{-1}). Absolute values of the capacitive peaks: j_1' = 7 μA cm^{-2}, j_2' = 21 μA cm^{-2}, j_3' = 49 μA cm^{-2}, and j_4' = 111 μA cm^{-2}. (d) Peak current versus the scan rate extracted from (c).

RHE), the cathodic peak is almost negligible. This indicates that traps are either totally filled by electrons and emptied by hole trapping when applying a high positive bias or created by oxidation of the hematite surface at higher voltage. As already discussed elsewhere, in the case of hematite, traps are formed by forcing the oxidation of the hematite surface by applying a sufficiently positive voltage.[24] After a pretreatment of one sun illumination at the potential V_0 = 1.66 V versus RHE, the cathodic peak height increases with scan rate, Figure 1c. Note that the voltammetry sweep is not performed under illumination in order to avoid masking the trap capacitive effects by the photocurrent. The voltage of the peak is shifted in the cathodic direction when the scan rate increases, as indicated by the gray arrow. The dependence of the cathodic peak current with scan rate is linear, as shown in Figure 1d, indicating that diffusion limitations do not exist for these experiments. It should also be noticed that under dark conditions at V_0 = 1.66 V versus RHE and at a scan rate of 500 mV/s (Figure 1a), the cathodic capacitive peak is hardly visible, while under illumination, the peak is visible even at 50 mV/s.

The previous observations indicate that traps are created chemically by oxidation of the hematite surface either by imposing a higher positive bias or by illumination. It has been suggested that these surface traps are Fe=O intermediates and the formation of these species by proton-coupled oxidation of surface hydroxide species constitutes the first step of water oxidation on hematite electrodes.[16,25] In other materials, like GaN for instance,[26] surface traps are mainly due to the morphology of the material and are present in the dark and under illumination. Consequently, in the latter situation, the voltammetry plots display a comparable capacitive peak for both pretreatments. Additionally, it should also be noted that no anodic peak is present in any of the plots represented in Figure 1a and c. However, it has been recently remarked[23] that after deposition of an iridium-based catalyst to the hematite surface, a quasi-symmetric peak can be observed at cathodic potentials, as depicted by Figure 2. This peak, which is observed

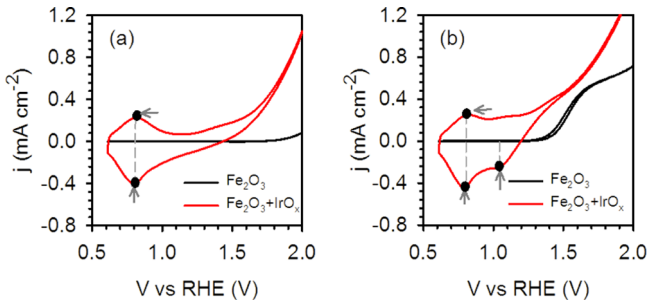

Figure 2. Cyclic voltammetry curves obtained in the dark (peak voltage: V_1 = 0.8V versus RHE; capacitive peaks: j_1^{cat} = −0.4 mA cm^{-2}, j_1^{an} = 0.22 mA cm^{-2}) (a) and under illumination at 100 mW cm^{-2} (second peak voltage: V_2 = 1.01 V versus RHE; cathodic peak: j_2^{cat} = −0.26 mA cm^{-2}) (b) for a reference Fe_2O_3 sample (black curve) and after electrodeposition of an IrO_x layer from a metallorganic [Cp*Ir$(H_2O)_3$](SO_4) precursor (red curve). Surface concentration of Ir on Fe_2O_3: 3.9 atom %. Scan rate: 10 mV s^{-1}.[23]

both in the dark and under illumination conditions, indicates that IrO_x acts in a similar fashion as intrinsic surface states, by capture and release of carriers from those states, which facilitates charge transfer to solution. This capacitive feature of IrO_x can be obviously related to the standard CV behavior of redox species. More specifically, it has been ascribed to an Ir(III)/Ir(IV) redox process, which involves a two-electron, three-proton process.[27,28] However, it is interesting to discuss how the redox catalyst is electronically coupled to the semiconductor film. Similar observations have been reported with cobalt−phosphate (Co−Pi) catalyst layers covering hematite electrodes.[15]

In the following, we present a simple model that allows prediction of the voltammetry plots in the presence of a monoenergetic level of surface states with a pretreatment done under illumination at a voltage above the onset voltage. The model, which is based on a previous model developed by Bisquert,[29] allows prediction of the voltammetry patterns reported in the present study and, in general, in the measurement of solar water splitting semiconductor films.

We consider a thin and homogeneous semiconductor film of length d with a density of N_t monoenergetic traps per unit of volume, as shown in Figure 3. We term n and f the density of electrons in the conduction band and the traps occupation probability, respectively. n_0 and f_0 are the same respective quantities taken at equilibrium. The detailed calculation of f_0 is given in the Supporting Information (SI). Because the distribution of carriers in the semiconductor layer is assumed to be homogeneous, n only depends on time and is governed by the applied voltage V

$$n(t) = n_0 \exp\left(-\frac{qV(t)}{k_B T}\right) \quad (1)$$

where $k_B T$ is the thermal energy.

dx.doi.org/10.1021/jz400573t | J. Phys. Chem. Lett. 2013, 4, 1334−1339

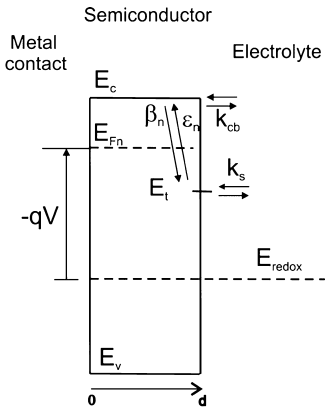

Figure 3. Scheme of the kinetics of the processes occurring at the interface of the semiconductor/solution. d is the thickness of the semiconductor layer. The processes are trapping of electrons from the conduction band (β_n) and detrapping (ε_n) and charge transfer of electrons from the traps (k_s) and from the conduction band (k_{cb}).

It is well-known that the presence of an electric field in the space charge region improves charge separation in the active layer, which can enhance the fuel production efficiency.[12] In the model below, we address the question of trap occupation and charge transfer from the surface states, depending on the homogeneous electrode potential. The same model could be formulated for a surface Schottky barrier with simple modifications, but these considerations are beyond the scope of this work. Henceforth, for the sake of simplicity, the influence of the electric field at the electrolyte/semiconductor interface is neglected.

Initially, before the voltammetry scan, a pretreatment is done in order to fill the traps with holes at a fixed voltage V_0 more positive than the current onset voltage. Therefore, when the voltammetry sweep starts, that is, at $t = 0$, we consider that $f(t{=}0) = 0$. For a more complete treatment, $f(t{=}0)$ should be calculated by taking into account both electron and hole recombination and charge transfer from traps. However, for simplicity, the dynamics of holes are not included in Figure 3. For the interested reader, such calculations can be found in ref 20 for the technique of IS.

During the cyclic voltammetry scan, that is, at time $t > 0$, the semiconductor is in the dark. Two types of processes are considered in this case, (i) charge transfer from the conduction band (kinetic constant k_{cb}) and from the traps (k_s) and (ii) electron trapping (β_n)/detrapping (ε_n). We aim to calculate the current density j_n, and we use the usual boundary conditions, eq 1 at the left metal/semiconductor contact, and at the right, the semiconductor/electrolyte contact is considered to be a blocking layer (i.e., $j_n(d,t) = 0$). The voltage that appears in eq 1 varies with time as

$$\begin{cases} V(t \le \lambda) = V_0 - st \\ V(t \ge \lambda) = V_0 - 2s\lambda + st \end{cases} \tag{2}$$

where s is the scan rate and λ the semi-period of the voltage sweep.

Integration of the continuity equation for electrons in the conduction band and the master equation for electrons in the traps along the homogeneous layer of length d leads to

$$\frac{\partial n}{\partial t} = -\frac{1}{qd} j_n(0) - \beta_n(1-f)nN_t + \varepsilon_n f N_t - k_{cb}(n - n_0) \tag{3}$$

$$\frac{\partial f}{\partial t} + \varepsilon_n + k_s(1 - f_0) = (\beta_n n + \varepsilon_n + k_s)(1 - f) \tag{4}$$

We shall introduce some useful quantities, namely, the equilibrium chemical capacitances[30,31] associated with each charge storage mode. We define the well-known chemical capacitance for electrons in the conduction band

$$C_\mu^{cb} = qd\left|\frac{\partial n}{\partial V}\right| = \frac{q^2 d}{kT} n \tag{5}$$

and the equilibrium chemical capacitance of the traps[32−34]

$$C_{\mu eq}^{ss} = qd\left|\frac{\partial f}{\partial V}\right| N_t \tag{6}$$

Note that the latter capacitance relies on the knowledge of f, which relies on the resolution of eq 4. Equations 2−4 provide the general form of the voltammetric current

$$\begin{cases} j_n(t \le \lambda) = j_{res} - j_{cap} \\ j_n(t \ge \lambda) = j_{res} + j_{cap} \end{cases} \tag{7}$$

where j_{res} is the resistive current density (i.e., faradaic current)

$$j_{res} = -qd\left[k_{cb} + (1 - B)\varepsilon_n \frac{N_t}{n_0} f_0\right] \times (n - n_0) \tag{8}$$

with

$$B = 1 - \frac{k_s}{\beta_n n + \varepsilon_n + k_s} \tag{9}$$

j_{cap} is the capacitive current density given by

$$j_{cap} = [C_\mu^{cb} + BC_{\mu eq}^{ss}] \times s \tag{10}$$

The first term on the right-hand side of eq 8 corresponds to the charge transfer from the conduction band, while the second term has already been associated through IS to the trapping/detrapping process and charge transfer from the traps.[29]

The general solution of the above set of equations can be obtained numerically, but it is useful to distinguish between different physical cases. In the model of Figure 3, we will consider that charge transfer from the traps is slow enough compared to the velocity of trap charging so that a capacitance peak can be observed. This implies that $k_s \ll qs/k_BT$. Note that in the case where charge transfer from the traps is zero ($k_s = 0$), the following treatment can also be applied for the bulk of the semiconductor if it is homogeneous enough so that eqs 3 and 4 remain valid. However, this latter case is not desired for fuel production because it would imply high onset voltages. Besides, as indicated by the experimental CV patterns of Figures 1 and 2, it is important to distinguish two types of behaviors; either trapping/detrapping is fast enough in comparison with the trap charging velocity, that is, $\varepsilon_n \gg qs/k_BT$ or inversely.

In the case where trapping/detrapping is very fast, traps are in equilibrium with the semiconductor conduction band, while in the second case, electrons accumulate in the traps and are therefore subject to much higher recombination. In the first case, the onset voltage should therefore be lower than that in

dx.doi.org/10.1021/jz400573t | J. Phys. Chem. Lett. 2013, 4, 1334−1339

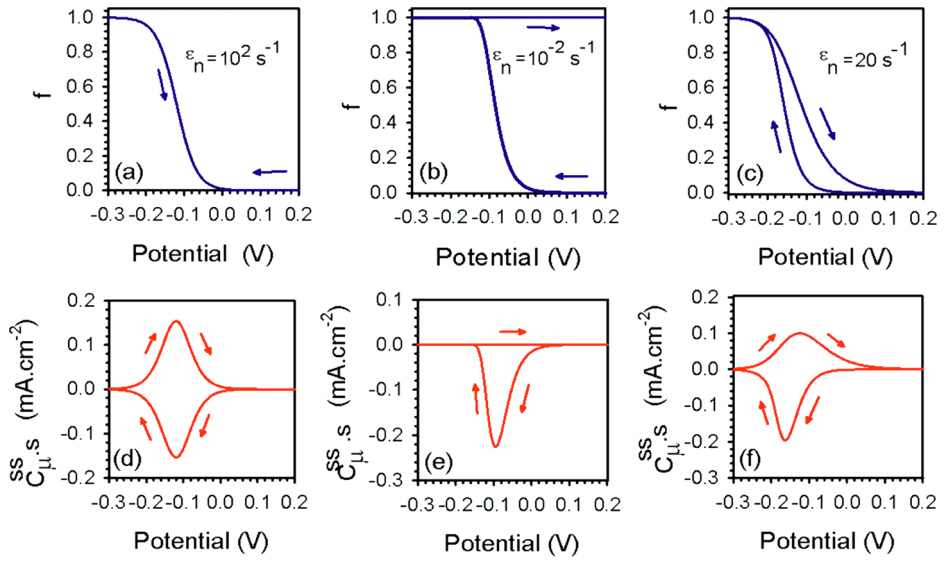

Figure 4. Trap occupation probability for a system limited by charge transfer and (a) when detrapping is fast with respect to the charging velocity (i.e., traps are in equilibrium with the conduction band), (b) when detrapping is slow (i.e., high recombination), and (c) for an intermediate case. (d–f) Trap capacitive current (C_μ^{ss}·s) derived from the respective occupation probability of (a–c). Simulation parameters: kT = 26 meV, d = 1 nm, $N_t = 10^{21}\ cm^{-3}$, $\beta_n n_0 = 1\ s^{-1}$, $k_s = 10^{-4}\ s^{-1}$, $s = 1\ V{\cdot}s^{-1}$.

the second one. Let us now examine both cases in terms of the voltammetry pattern and relate them to the experimental cases depicted by Figures 1 and 2.

In Figure 4, we give examples of representation of the trap occupation probability f for a system limited by charge transfer. We illustrate three cases, when detrapping is fast, depicted in Figure 4a, when detrapping is slow, shown in Figure 4b, and an intermediary case represented in Figure 4c. The corresponding capacitive currents (C_μ^{ss}·s) from the traps are given in Figure 4d–f. In Figure 5, we give the total voltammetric current obtained from the numerical resolution of eqs 3 and 4 corresponding to the same cases as in the top row.

We now discuss the influence of the trap kinetics on the voltammetry patterns for semiconductors used for water splitting applications. We focus on the possible shapes of the CV patterns obtained in the framework of our model. We then compare them to both experimental examples of Figures 1 and 2, which are representative of the main voltammetry plots that can be found in the literature for this type of system.

When the voltammetry scan is carried out in the cathodic direction, the electron Fermi level is shifted upward, and traps (initially filled with holes because of the pretreatment) are filled with electrons while the conduction band is filled at more cathodic voltage. The voltammetry pattern therefore displays a first cathodic capacitive peak induced by the filling of the traps by electrons followed either by the faradic current from the conduction band (Figure 5b and d) or by the capacitive current (Figures 5a and c). In the anodic direction, because charge transfer from the traps is slow with respect to the trap charging velocity, traps are emptied relatively according to the detrapping rate.

In the case where detrapping is very slow (Figure 5a and b) with respect to the trap charging velocity, charges accumulate in the traps in the cathodic direction. Note that in this case, the voltage of the cathodic peak depends on the scan rate and is shifted toward the cathodic direction as the scan rate increases. The mathematical demonstration of this result is given in the SI. In the anodic direction, because detrapping is very slow, the charges accumulated in the traps are extracted much slower

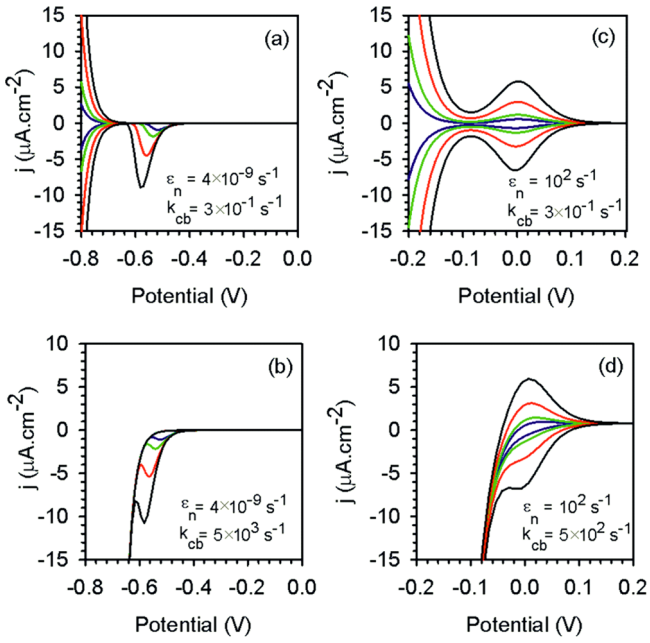

Figure 5. Voltammetric plots obtained by solving numerically eqs 3 and 4 under the condition that charge transfer is a limiting kinetic factor. Four different cases are computed where detrapping ($\varepsilon_n = \beta_n n_0$) and charge transfer from the conduction band (k_{cb}) are analyzed. The general parameters of this simulation are kT = 26 meV, d = 1 nm, $N_t = 8 \times 10^{19}\ cm^{-3}$, $k_s = 10^{-2}\ s^{-1}$. For each figure, the blue plot corresponds to the scan rate 50 mV·s^{-1}, the green plot to 100 mV·s^{-1}, the red plot to 250 mV·s^{-1}, and the black one to 500 mV·s^{-1}.

than they were injected in the cathodic direction. For this reason, the occupation probability is almost constant and maximum in the anodic direction (Figure 4b). As a consequence, no anodic peak can be observed. Experimentally, this latter case is depicted by Figure 1 for bare hematite. In this case, traps are formed by oxidation of the hematite surface. The shape of the capacitive peak that appears after illumination of the sample indicates that not only is the charge transfer from

dx.doi.org/10.1021/jz400573t | J. Phys. Chem. Lett. 2013, 4, 1334–1339

the traps slow, but also, the detrapping process is sluggish. Thereby, traps actuate as recombination centers and limit the oxygen evolution. The same behavior has been reported in the case of GaN.[26] Nonetheless, in this case, surface states are intrinsic and display a capacitive peak in both dark and illumination conditions, though the peak intensity is higher under illumination compared to that under dark conditions. This is due to the fact that in the dark, those surface states are initially partially filled with electrons, while under illumination, traps are emptied by hole trapping, which allows for higher charge accumulation during the voltammetry sweep.

In the case where both trapping and detrapping are fast compared to the trap charging velocity (Figure 5c and d), charge accumulation is reversible, and the occupation probability is equal in both the anodic and cathodic directions (Figure 4a). Hence, the trap capacitance is the same in both directions, and the trap capacitive current is symmetric and proportional to the scan rate (see the SI for more information on the capacitance peak voltage). This situation corresponds to the experimental case depicted by Figure 2. When the hematite surface is treated with an iridium-based catalyst, two quasi-symmetric peaks, cathodically shifted with respect to the bare hematite peak, appear under both dark and illumination conditions. This indicates that IrO_x highly reversible oxidation states act similarly to intrinsic surface states and that detrapping is much easier in this case. Consequently, the IrO_x catalyst enhances the detrapping process and decreases recombination. For this reason, higher currents and lower onset voltages can be achieved.[35] It has also been shown by IS that IrO_x enhances charge transfer.[23] Additionally, it should be remarked that a second cathodic peak appears under illumination. We believe that this peak corresponds to the surface states created by oxidation of the hematite surface, as already observed for bare hematite. It should also be remarked that in other recent studies, the capacitive response of surface states has been found to be reduced in the presence of Ga_2O_3 and Al_2O_3 overlayers.[36,37] It has been suggested that 13-group oxide overlayers passivate surface states by releasing lattice strain of the hematite layer. On the other hand, the deposition of cobalt-based catalyst layers also leads to a decrease of surface state capacitance by accelerating the charge-transfer rate from surface states.[38] It should be mentioned that these previous studies were carried out under illumination, and consequently, the capacitive response of the electrodes was partially masked by the photocurrent, in contrast with our present study in dark conditions.

In conclusion, we have shown that when charge transfer is very slow, at least one capacitive peak can be observed in the voltammograms corresponding to the system at stake. The presence of one capacitive peak only in the cathodic direction (i.e., without the corresponding symmetric anodic peak) is a feature of a system exhibiting high recombination. In this case, the peak voltage is shifted in the cathodic direction as the scan rate increases. On the contrary, two symmetric peaks characterize a system with trap states in equilibrium with the conduction band and display lower recombination compared to the previous case. In this case, both peaks increase proportionally to the scan rate, and the peak voltage is constant with scan rate. A system that is characterized by a good charge transfer from traps does not display any capacitive peak.

■ ASSOCIATED CONTENT

Ⓢ Supporting Information

The detailed calculation of the trap occupation probability at equilibrium and the capacitance peak voltage observed in the CV patterns in both cases of slow and fast trapping/detrapping with respect to the trap charging velocity. This material is available free of charge via the Internet at http://pubs.acs.org.

■ AUTHOR INFORMATION

Corresponding Author

*E-mail: bisquert@uji.es.

Notes

The authors declare no competing financial interest.

■ ACKNOWLEDGMENTS

The research leading to these results is supported by Universitat Jaume I Project P1·1B2011-50.

■ REFERENCES

(1) Bolts, J.; Wrighton, M. Correlation of Photocurrent−Voltage Curves with Flat-Band Potential Stable Photoelectrodes for the Photoelectrolysis of Water. *J. Phys. Chem.* **1976**, *80*, 2641−2645.

(2) Nozik, A. J. Photoelectrochemistry: Applications to Solar Energy Conversion. *Annu. Rev. Phys. Chem.* **1978**, *29*, 189.

(3) Butler, M. A.; Ginley, D. S. Principles of Photoelectrochemical, Solar Energy Conversion. *J. Mater. Sci.* **1980**, *15*, 1−19.

(4) Walter, M. G.; Warren, E. L.; McKone, J. R.; Boettcher, S. W.; Mi, Q. X.; Santori, E. A.; Lewis, N. S. Solar Water Splitting Cells. *Chem. Rev.* **2010**, *110*, 6446−6473.

(5) Kennedy, J. H. Photooxidation of Water at α-Fe_2O_3 Electrodes. *J. Electrochem. Soc.* **1978**, *125*, 709.

(6) Murphy, A.; Barnes, P.; Randeniya, L.; Plumb, I.; Grey, I.; Horne, M.; Glasscock, J. Efficiency of Solar Water Splitting Using Semiconductor Electrodes. *Int. J. Hydrogen Energy* **2006**, *31*, 1999−2017.

(7) Dare-Edwards, M. P.; Goodenough, J. B.; Hamnett, A.; Trevellick, P. R. Electrochemistry and Photoelectrochemistry of Iron(III) Oxide. *J. Chem. Soc., Faraday Trans. 1* **1983**, *79*, 2027−2041.

(8) Katz, M. J.; Riha, S. C.; Jeong, N. C.; Martinson, A. B. F.; Farha, O. K.; Hupp, J. T. Toward Solar Fuels: Water Splitting with Sunlight and Rust? *Coord. Chem. Rev.* **2012**, *256*, 2521−2529.

(9) Peter, L. M. Energetics and Kinetics of Light-Driven Oxygen Evolution at Semiconductor Electrodes: The Example of Hematite. *J. Solid State Electrochem.* **2012**, *17*, 315−326.

(10) Barroso, M.; Cowan, A. J.; Pendlebury, S. R.; Gratzel, M.; Klug, D. R.; Durrant, J. R. The Role of Cobalt Phosphate in Enhancing the Photocatalytic Activity of α-Fe_2O_3 toward Water Oxidation. *J. Am. Chem. Soc.* **2011**, *133*, 14868−14871.

(11) Zhong, D. K.; Choi, S.; Gamelin, D. R. Near-Complete Suppression of Surface Recombination in Solar Photoelectrolysis by "Co−Pi" Catalyst-Modified W:BiVO4. *J. Am. Chem. Soc.* **2011**, *133*, 18370−18377.

(12) Barroso, M.; Mesa, C. A.; Pendlebury, S. R.; Cowan, A. J.; Hisatomi, T.; Sivula, K.; Gratzel, M.; Klug, D. R.; Durrant, J. R. Dynamics of Photogenerated Holes in Surface Modified α-Fe_2O_3 Photoanodes for Solar Water Splitting. *Proc. Natl. Acad. Sci. U.S.A.* **2012**, *109*, 15640−15645.

(13) Wijayanthaa, K. G. U.; Saremi-Yarahmadia, S.; Peter, L. M. Kinetics of Oxygen Evolution at α-Fe_2O_3 Photoanodes: A Study by Photoelectrochemical Impedance Spectroscopy. *Phys. Chem. Chem. Phys.* **2010**, *13*, 5264−5270.

(14) Peter, L. M.; Wijayantha, K. G. U.; Tahir, A. A. Kinetics of Light-Driven Oxygen Evolution at α-Fe_2O_3 Electrodes. *Faraday Discuss.* **2012**, *155*, 309−322.

(15) Klahr, B.; Gimenez, S.; Fabregat-Santiago, F.; Bisquert, J.; Hamann, T. W. Photoelectrochemical and Impedance Spectroscopic

Investigation of Water Oxidation with Co−Pi-Coated Hematite Electrodes. *J. Am. Chem. Soc.* **2012**, *134*, 16693−16700.
(16) Klahr, B.; Gimenez, S.; Fabregat-Santiago, F.; Bisquert, J.; Hamann, T. W. Electrochemical and Photoelectrochemical Investigation of Water Oxidation with Hematite Electrodes. *Energy. Environ. Sci.* **2012**, *5*, 7626.
(17) Braun, A.; Sivula, K.; Bora, D. K.; Zhu, J.; Zhang, L.; Grätzel, M.; Guo, J.; Constable, E. C. Direct Observation of Two Electron Holes in a Hematite Photo-Anode During Photo-Electrochemical Water Splitting. *J. Phys. Chem. C* **2012**, *116*, 16870−16875.
(18) Vanmaekelbergh, D.; Cardon, F. Calculation of the Electrical Impedance Associated with the Surface Recombination of Free Carriers at an Illuminated Semiconductor/Electrolyte Interface. *J. Phys. D: Appl. Phys.* **1986**, *19*, 643.
(19) Ponomarev, E. A.; Peter, L. M. A Comparison of Intensity Modulated Photocurrent Spectroscopy and Photoelectrochemical Impedance Spectroscopy in a Study of Photoelectrochemical Hydrogen Evolution at p-InP. *J. Electrochem. Chem.* **1995**, *397*, 45−52.
(20) Bertoluzzi, L.; Bisquert, J. Equivalent Circuit of Electrons and Holes in Thin Semiconductor Films for Photoelectrochemical Water Splitting Applications. *J. Phys. Chem. Lett.* **2012**, *3*, 2517−2522.
(21) Fabregat-Santiago, F.; Mora-Seró, I.; Garcia-Belmonte, G.; Bisquert, J. Cyclic Voltammetry Studies of Nanoporous Semiconductor Electrodes. Models and Application to Nanocrystalline TiO_2 in Aqueous Electrolyte. *J. Phys. Chem. B* **2003**, *107*, 758−769.
(22) Kay, A.; Cesar, I.; Grätzel, M. New Benchmark for Water Photooxidation by Nanostructured α-Fe_2O_3 Films. *J. Am. Chem. Soc.* **2006**, *128*, 15714−15721.
(23) Badia-Bou, L.; Mas Marzá, E.; Rodenas, P.; Barea, E. M.; Fabregat-Santiago, F.; Gimenez, S.; Peris, E. V.; Bisquert, J. Water Oxidation at Hematite Photoelectrodes with an Iridium Based Catalyst. *J. Phys. Chem. C* **2013**, *117*, 3826−3833.
(24) Jaegermann, W. The Semiconductor/Electrolyte Interface: A Surface Science Approach. In *Modern Aspects of Electrochemistry*; White, R. E., Ed.; Plenum Press: New York, 1996; No. 30.
(25) Hellman, A.; Pala, R. G. S. A First-Principles Study of Photo-Induced Water-Splitting on Fe_2O_3. *J. Phys. Chem. C* **2011**, *115*, 12901−12907.
(26) Schäfer, S.; Koch, A. H. R.; Cavallini, A.; Stutzmann, M.; Sharp, I. D. Charge Transfer across the n-Type GaN−Electrolyte Interface. *J. Phys. Chem. C* **2012**, *116*, 22281−22286.
(27) Blakemore, J. D.; Schley, N. D.; Olack, G. W.; Incarvito, C. D.; Brudvig, G. W.; Crabtree, R. H. Anodic Deposition of a Robust Iridium-Based Water-Oxidation Catalyst from Organometallic Precursors. *Chem. Sci.* **2011**, *2*, 94−98.
(28) Burke, L. D.; Whelan, D. P. A New Interpretation of the Charge Storage and Electrical-Conductivity Behavior of Hydrous Iridium Oxide. *J. Electroanal. Chem.* **1981**, *124*, 333−337.
(29) Bisquert, J. Theory of the Impedance of Charge Transfer via Surface States in Dye-Sensitized Solar Cells. *J. Electrochem. Chem.* **2010**, *646*, 43−51.
(30) Bisquert, J. Chemical Capacitance of Nanostructured Semiconductors: Its Origin and Significance for Heterogeneous Solar Cells. *Phys. Chem. Chem. Phys.* **2003**, *5*, 5360−5364.
(31) Bisquert, J. Beyond the Quasi-Static Approximation: Impedance and Capacitance of an Exponential Distribution of Traps. *Phys. Rev. B* **2008**, *77*, 235203.
(32) Frese, K. W.; Morrison, S. R. Electrochemical Measurements of Interface States at the GaAs/Oxide Interface. *J. Electrochem. Soc.* **1979**, *126*, 1235−1241.
(33) Dare-Edwards, M. P.; Hamnett, A.; Trevellick, P. R. Alternating-Current Techniques in Semiconductor Electrochemistry. *J. Chem. Soc., Faraday Trans. 1* **1983**, *79*, 2111−2124.
(34) Allongue, P.; Cachet, H. I−V Curve and Surface State Capacitance at Illuminated Semiconductor/Liquid Contacts. *J. Electrochem. Chem.* **1984**, *176*, 369−375.
(35) Tilley, S. D.; Cornuz, M.; Sivula, K.; Gratzel, M. Light-Induced Water Splitting with Hematite: Improved Nanostructure and Iridium Oxide Catalysis. *Angew. Chem., Int. Ed.* **2010**, *49*, 6405−6408.
(36) Le Formal, F.; Sivula, K.; Grätzel, M. The Transient Photocurrent and Photovoltage Behavior of a Hematite Photoanode under Working Conditions and the Influence of Surface Treatments. *J. Phys. Chem. C* **2012**, *116*, 26707−26720.
(37) Hisatomi, T.; Le Formal, F.; Cornuz, M.; Brillet, J.; Tetreault, N.; Sivula, K.; Gratzel, M. Cathodic Shift in Onset Potential of Solar Oxygen Evolution on Hematite by 13-Group Oxide Overlayers. *Energy Environ. Sci.* **2011**, *4*, 2512−2515.
(38) Riha, S. C.; Klahr, B. M.; Tyo, E. C.; Seifert, S.; Vajda, S.; Pellin, M. J.; Hamann, T. W.; Martinson, A. B. F. Atomic Layer Deposition of a Submonolayer Catalyst for the Enhanced Photoelectrochemical Performance of Water Oxidation with Hematite. *ACS Nano* **2013**, *7*, 2396−2405.